Published in final edited form as:
Polyhedron. 2014 March 9; 70: 29–38. doi:10.1016/j.poly.2013.12.019.

A combined experimental and theoretical study of dinitrosyl iron complexes containing chelating bis(diphenyl)phosphinoX (X = benzene, propane and ethylene): X-ray crystal structures and properties influenced by the presence or absence of π-bonds in chelating ligands

Lauren R. Holloway[a], **Andrew J. Clough**[a], **Jessica Y. Li**[b], **Emily L. Tao**[b], **Fu-Ming Tao**[b,*], and **Lijuan Li**[a,*]

[a]Department of Chemistry and Biochemistry, California State University, Long Beach, 1250 Bellflower Blvd., Long Beach, CA 90840 USA

[b]Department of Chemistry and Biochemistry, California State University, Fullerton, P.O. Box 6866, Fullerton, CA 92834 USA

Abstract

Recent discoveries involving the roles of nitric oxide in humans have stimulated intense interest in transition metal nitrosyl complexes. A series of dinitrosyl iron complexes with the formula $[(DPPX)Fe(NO)_2]$, {DPPX = 1,2-bis(diphenylphosphino)benzene (**1**), 1,3-bis(diphenylphosphino)propane (**2**), and cis-1,2-bis(diphenylphosphino)ethylene (**3**)} has been prepared and characterized through a combination of FT-IR, NMR, UV-vis, X-ray crystallography, and electrochemical techniques. Infrared spectroscopy showed NO shifts to the region of 1723 and 1674 cm^{-1} for complexes **1** and **3**, and 1708 and 1660 cm^{-1} for **2**, indicating that ligand **2** acts as a stronger σ–donor. The X-ray crystallographic data showed that **1** and **3** possess the rare *repulso* conformation while **2** has the *attracto* conformation. CV studies on compounds **1**, **2** and **3** display two quasi-reversible oxidations with the $E°_{1/2}$ values at 0.101 and 0.186 V, 0.121 and 0.184 V, and 0.019 and 0.342 V, respectively. The larger ΔE value for compound **2** compared with that of **1** and **3** is attributed to the lack of π-bonds between the two phosphorus atoms. Theoretical calculations using density functional theory were carried out on the synthesized compounds and model compounds and the results are consistent with the experimental data. The calculated HOMO-LUMO gaps for compounds **1, 2** and **3** are 3.736, 4.060, and 3.669

*To whom correspondence should be addressed. [a]L.L.: tel, (562) 985-5068; lli@csulb.edu. [b]F.M.T.: tel, (657) 278-4517; ftao@exchange.fullerton.edu.

Appendix A. Supplementary data

CCDC 965700, 965701 and 965702 contain the supplementary crystallographic data for compounds **1**, **2** and **3**. These data sets can be obtained free of charge via http://www.ccdc.cam.ac.uk/conts/retrieving.html, or from the Cambridge Crystallographic Data Centre, 12 Union Road, Cambridge CB2 1EZ, UK; fax: (+44) 1223-336-033; or e-mail: deposit@ccdc.cam.ac.uk.

eV, respectively, which supports the stronger back-donation for compound **2** than that of compounds **1** and **3**.

Keywords

dinitrosyl iron complexes; chelating bisphosphines; spectroscopy; DFT calculations

Introduction

The realization that nitric oxide (NO) is a biological messenger in many physiological processes has brought about a renewed interest in its chemistry, particularly the iron complexes that are central to the role of nitric oxide within the body.[i] Specifically, non-heme iron nitrosyl complexes have been identified as the products of biosynthetic evolution of NO, suggested as a means of NO storage, and found to be responsible for several important biological functions.[ii] Among those, dinitrosyl iron complexes (DNICs) have also been identified in the macrophages responsible for killing invading microorganisms by releasing NO.[iii] They are also found to be cytotoxic to *E-coli* bacteria[iv] and some of them exhibit anti-tumor activities.[v] These discoveries have stimulated intense interest in isolating and studying metal-nitrosyl complexes, especially those that mimic the structures of biologically active non-heme iron nitrosyl complexes,[vi] and those capable of releasing NO for pharmacological and medicinal applications.[vii]

Bidentate phosphine ligands are commonly used in organic chemistry as activators for catalyst complexes. Coordination complexes of triphenylphosphine, chelating agents such as 1,2-bis(diphenylphosphino)ethane or 1,1-bis(diphenylphosphino) methane are generally used as homogeneous catalysts for a wide range of reactions. These catalysts frequently make use of transition metals like palladium and iridium.[viii] A few examples of phosphine disubstituted nitrosyl complexes have been previously synthesized as early as 1962 with some recent examples reported as well.[ix] However the vast majority of these compounds are not chelated species and crystallographic data was not provided, nor was a detailed analysis of the compounds done.[x]

In continuing our interest in the preparation of novel dinitrosyl iron complexes, we have reported chelating compounds using N,N-chelating ligands,[xi] and dinuclear dinitrosyliron complexes linked by bis(diphenyl)phosphine ligands.[xii] In this paper, reactions using $Fe(NO)_2(CO)_2$ and a series of bis(diphenylphosphine) chelating ligands ranging in sizes and the presence or absence of **π**-bonds in the carbon backbones, such as 1,2-bis(diphenyl-phosphino)benzene, (DPPBz), 1,3-bis(diphenylphosphino)propane, (DPPP), and cis-1,2-bis(diphenylphosphino)ethylene, (DPPEt) were investigated. From these reactions, three chelated products with the general formula $[(DPPX)Fe(NO)_2]$, where DPPX = $C_6H_4[P(C_6H_5)_2]_2$, $(C_6H_5)_2PCH_2CH_2CH_2P(C_6H_5)_2$, and $(C_6H_5)_2PCH{=}CHP(C_6H_5)_2$ were isolated and characterized using methods such as FT-IR, UV-Vis, and NMR spectroscopies as well as X-Ray crystallography and cyclic voltammetry. Quantum mechanical calculations using density functional theory were performed on these compounds and their model

compounds using two different methods. The calculated results were found to be consistent with the experimental observations.

Materials and Methods

All solvents were purchased from Aldrich in anhydrous form or obtained dry and air free from a MBRAUN MB-SPS dispenser (Manual Solvent Purification System) and stored in small amounts over 3 or 4 Å molecular sieves. Pentacarbonyliron(0), 1,2-bis(diphenylphosphino)benzene (DPPBz), *cis*-1,2-bis(diphenylphosphino)ethylene (DPPEt), and 1,3-bis(diphenylphosphino)propane (DPPP) were all purchased from Sigma Aldrich and used without further purification. Dicarbonyldinitrosyliron(0) was synthesized using a modified method of Seel's procedure.[xiii,xiv] Because the $Fe(CO)_2(NO)_2$ is very volatile and tends to decompose over time, it was stored in individual 1 mL aliquots as a 1:1 solution with dichloromethane or THF for a later use.

Synthesis of $Fe(NO)_2$(DPPBz) (1)

1,2-Bis(diphenylphosphino)benzene (DPPBz) ligand (0.405 g, 0.907 mmol) was dissolved in a minimal amount of THF (no more than 7 mL) in a glovebox at room temperature with stirring in a 25 mL round bottom flask fitted with a rubber septum. Then 0.2 mL (0.0907 mmol) of $Fe(CO)_2(NO)_2$/THF solution (1:1 ratio) was introduced into the flask via syringe. The solution was allowed to stir at room temperature overnight to produce the monosubstituted product, $Fe(NO)_2(CO)$(DPPBz). After stirring, the reaction mixture was taken out of the glovebox and gently heated at 50°C for 24 hours with the reaction progress monitored through FT-IR spectroscopy. The solution was transferred back into the glovebox after completion of the double substitution. Large dark purple crystals of X-ray quality ranging in size from 0.5 mm^3 to 3 mm^3 were grown by allowing the solvent to slowly evaporate over several days through a vent needle. The crystals and solid powder from the bottom of the flask were filtered and washed with three 0.5 mL aliquots of cool toluene. Yield: 0.343g, 72%; IR (in THF) $\nu_{(NO)}$ (cm^{-1}): 1719 and 1675. NMR (δ-ppm): ^{1}H, 7.170 (s) and 7.323 (d, J = 7.8 Hz) (C_6H_5), 7.546 (m) (C_6H_4); ^{13}C, 126.0 (s, p-C_6H_5), 128.8 (s) and 129.6 (s) (o- or m-C_6H_5), 133.4 (t, $J_{C\text{-}P}$ = 6.4 Hz) and 129.1 (t, $J_{C\text{-}P}$ = 5.1 Hz) (ipso-C_6H_5 or C_6H_4), 138.4 (s) and 130.6 (s) (o- or m-C_6H_4). Elemental analysis: Expt (calc): C, 51.47% (64.08%); H, 4.10% (4.30%); N, 3.72% (4.98%).

Synthesis of $Fe(NO)_2$(DPPP) (2)

Synthesis of the chelated species was done by adding 0.374 g (0.907 mmol) of 1,3-bis(diphenylphosphino)propane (DPPP) to 10 mL THF at room temperature with stirring under a nitrogen atmosphere in a 50 mL round bottom flask with a rubber septum. Then 0.2 mL (0.0907 mmol) of a 1:1 $Fe(CO)_2(NO)_2$/THF solution was introduced into the flask via syringe. The solution was allowed to stir at room temperature overnight to obtain the monosubstituted product, $Fe(NO)_2(CO)$(DPPP). After stirring, the reaction mixture was transferred out of the glovebox and gently heated at 50°C. IR analysis of the liquid phase showed a sharp decrease in the intensity of the remaining CO peak after 24 hours and very little change in the intensity after 36 hours of heating. The mixture was transferred into the glovebox where the solvent was allowed to slowly evaporate. Small needle-shaped red

crystals of X-ray quality ranging in size from 0.5mm^3 to 1mm^3 were grown by allowing the solvent to slowly evaporate over several days. The crystals and solid powder from the bottom of the flask were filtered and washed with three 0.5 mL aliquots of cool toluene. Yield: 0.302g, 63%; IR (in CH_2Cl_2) $\nu_{(NO)}$ (cm^{-1}): 1708 and 1660. NMR (δ-ppm): ^{1}H, 2.027 (m) and 2.427 (m, J_{H-P} = 10.8 Hz, J_{H-H} = 7.8 Hz) ($CH_2CH_2CH_2$), 7.272 (m) and 7.455 (m) (20 H, C_6H_5); ^{13}C, 20.3 (s) (-CH_2-), 28.7 (d, J_{C-P} = 2.5 Hz) (CH_2-R-CH_2), 135.4 (doublet of doublets, $J_{C-P(1)}$ = 33.2 Hz, $J_{C-P(2)}$ = 2.7 Hz) (ipso-C_6H_5), 128.5 (d, J_{C-P} = 12.7 Hz) and 132.2 (d, J_{C-P} = 10.0 Hz) (o- or m-C_6H_5), 129.8 (s) (p-C_6H_5). Elemental Analysis: Expt (calc) C, 61.70% (61.38%); H, 5.01% (4.96%); N, 5.19% (5.30%).

Synthesis of $Fe(NO)_2$(DPPEt) (3)

In order to synthesize the chelated product, 0.359 g (0.907 mmol) of (*cis*-1,2-bis(diphenylphosphino)ethylene) DPPEt was dissolved in 10 mL THF at room temperature under a nitrogen atmosphere in a 50 mL round bottom flask with a rubber septum. Then, 0.2 mL (0.0907 mmol) of a 1:1 $Fe(CO)_2(NO)_2$/THF solution was introduced into the flask via syringe. The solution was allowed to sit at room temperature overnight. IR analysis showed the presence of only one CO stretching peak, indicating the loss of one of the carbonyls and substitution with one of the phosphine groups. The flask was transferred out of the glovebox and gently heated at 50°C for 24 hrs. IR analysis of the liquid phase showed a sharp decrease in the intensity of the remaining CO peak after 24 hrs and very little change in the intensity after 36 hrs of heating. The mixture was transferred inside the glovebox where the solvent was allowed to slowly evaporate. Large dark purple plate crystals of X-ray quality ranging in size from 1 mm^3 to 5 mm^3 were grown by allowing the solvent to slowly evaporate over several days. The crystals and solid powder from the bottom of the flask were filtered and washed with three 0.5 mL aliquots of cool toluene. Yield: 0.353g, 76%; IR (in CH_2Cl_2) $\nu_{(NO)}$ (cm^{-1}): 1723 and 1674. NMR (δ-ppm): ^{1}H, 7.436 (m) (20H, C_6H_5), 7.738 (2H, CH=CH); ^{13}C, 134.5 (d, J_{C-P} = 21.2 Hz) (ipso-C_6H_5), 132.2 (t, J_{C-P} = 6.4 Hz) and 128.9 (t, J_{C-P} = 5.1 Hz) (o- or m-C_6H_5), 130.3 (s) (p-C_6H_5), 148.8 (t, J_{C-P} = 33.6 Hz) (CH=CH). Elemental analysis: Expt (calc): C, 59.74% (60.96%); H, 4.40% (4.33%); N, 5.09% (5.47%).

Spectroscopic Measurements

All Solid and liquid Fourier Transform Infrared (FT-IR) spectra were recorded on a Nicolet FT-IR iS10 spectrometer using the Smart MIracle ZnSe ATR Accessory with a ZnSe crystal or a Smart OMNI-Transmission accessory with KBr pellets in the range of 400–4000 cm^{-1}. Air sensitive solids and liquids were prepared in the glovebox and scanned using the Smart OMNI-Transmission accessory under a dry nitrogen environment. ^{1}H and ^{13}C NMR spectra were recorded on a Bruker 300 MHz NMR spectrometer, using tetramethylsilane as an internal standard. NMR samples were prepared in the glove box under nitrogen by dissolving an appropriate amount of product in 0.5 ml of deuterated solvent and filtering any undissolved sample through glass wool. The UV-Visible absorption spectra were recorded on a Shimadzu UV-2100U spectrophotometer. The samples were prepared inside a glovebox under a nitrogen atmosphere using Quartz airtight cells with anhydrous dichloromethane as a solvent.

X-ray crystallography

X-ray crystallographic data for complexes **1**, **2** and **3** were collected from a single crystal sample mounted on a glass fiber. The instrument used for the diffraction data collection was a Bruker SMART APEX II diffractometer equipped with a fine focus, 2.0kW sealed tube X-ray source (MoKα radiation, λ = 0.71073Å) operating at 50kV and 30mA. Data collection was carried out by APEX II software. SAINT-PLUS was used to integrate the intensity of reflections, while SADABS was used for scaling and absorption correction. The structures were solved using the heavy atom method. All non-hydrogen atoms were refined anisotropically. Computations were performed using SHELXTL and final full-matrix refinements were against F^2.[xv]

Electrochemistry

The electrochemical studies were performed on a CH Instruments electrochemical analyzer 660A. A three-electrode system consisting of a platinum working electrode, a platinum wire counter electrode and an Ag/Ag^+ reference electrode was used. The reference electrode was separated from the bulk of the solution by a fritted-glass bridge filled with a solvent/ supporting electrolyte mixture. Cyclic voltammograms were recorded in a CH_2Cl_2 solution of 0.1 M tetrabutylammonium perchlorate (TBAP) with a sample concentration of approximately 0.001 M and a scan rate from 100 mVs^{-1} to 900 mVs^{-1}. A background spectrum was taken for each aliquot of electrolyte solution to ensure that the solvent and electrolyte had not become contaminated. The cyclic voltammogram of ferrocene was recorded each day before a set of experiments in order to counteract any drift from the reference electrode. The potential values are reported vs ferrocene/ferrocenium ion; the $E_{1/2[Fe(Cp)2/Fe(Cp)2^+]}$ under our experimental conditions is 0.132 V.

Theoretical calculations

The equilibrium geometries of the three compounds were calculated using density functional theory (DFT) with Becke's three-parameter exchange potential and the Lee-Yang-Parr correlation functional (B3LYP) along with the 6–31+G(d) basis set.[xvi] In order to confirm the convergence of the geometries with the basis set, additional B3LYP calculations using the aug-cc-pVDZ basis set as well as the 6–31+G(d) basis set were performed on the model systems representing the three compounds. In these model systems, methyl groups were used to replace the phenyl groups in the original compounds.

Harmonic frequency calculations were carried out for the three compounds and the model systems following geometry optimization in our calculations. All harmonic frequencies obtained were found to be real, confirming each of the equilibrium geometries calculated corresponded to a minimum on the potential energy surface. Additionally, some of the calculated harmonic frequencies, particularly the NO stretch frequencies, can be directly compared with the experimental frequencies. All calculations were carried out using the GAUSSIAN 09 computational chemistry program.[xvii]

Results and Discussion

Reactions

Compounds **1–3** were synthesized by first generating the corresponding monosubstituted compounds at room temperature and then heating the reaction mixture at 50°C for 24 – 36 hrs. Attempts to synthesize the chelated species through immediate heating of the reaction mixture without first producing the monosubstituted species lead to decomposition and overall loss of product. The general synthesis of the monosubstituted and chelated compounds is depicted in Scheme 1.

It has been reported that the reaction kinetics for the substitution of the first carbonyl can follow pseudo-first order kinetics,[xviii] therefore the rate of the reaction will be dependent on the concentration of the nucleophile. By introducing $Fe(CO)_2(NO)_2$ to the phosphine ligand in high concentrations (using a minimal amount of solvent to dissolve the ligand before injecting the starting material) the reaction yields nearly pure monosubstituted product in as little as one hour. The formation of the monosubstituted compounds was monitored using FT-IR spectroscopy in order to confirm that a shorter reaction time was possible under the new synthesis conditions. It was observed that the first CO group was almost entirely replaced within approximately 40 minutes.

The second carbonyl substitution occurs over a longer period of time when compared with the first. The chelation reaction itself depends on the orientation of the second phosphine group being correct to replace the second carbonyl. IR analysis of the solutions of the monosubstituted products shows that a small amount of the chelated species can form without the application of heat. This behavior was only observed in complexes **1** and **3** where the conjugated carbon bridge locks the phosphine in the correct orientation. This behavior is demonstrated by the presence of several downshifted NO peaks in the IR spectra of the compounds. The chelation process for these two complexes is only dependent on the rotation of the iron-phosphorus and phosphorus-carbon bonds of the ligand, and not on the rotation of the long saturated carbon chain present in the ligand of compound **2**.

The compounds **1–3** are insoluble in nonpolar organic solvents such as toluene and pentane but are moderately soluble in halogenated solvents like dichloromethane and chloroform. The monosubstituted complexes are highly air sensitive and will decompose rapidly, forming a black sticky solid upon being exposed to air. The chelated compounds appear to be air stable for up to 12 hours in the crystalline form. In a solution of dichloromethane, compounds **1** and **3** are stable for several days while compound **2** decomposes over 8 hours.

^{1}H and ^{13}C NMR spectroscopy showed well-resolved spectra and all complexes were found to be relatively pure, with the exception of compound **1**, where the NMR showed some solvent residues present from the synthesis. Coupling of carbons and protons to the phosphorous atoms at up to three bonds away was observed, and all carbons and protons have been identified in the spectra. Elemental analysis for **2** and **3** matches well with the theoretical one, except for compound **1**, possibly due to the presence of solvent as shown in NMR.

Infrared Spectroscopy

The synthesis of both monosubstituted and chelated compounds was qualitatively monitored through the use of IR spectroscopy to ensure the completion of the reactions. The loss of carbonyl stretching peaks is easily noted due to their usual intensity and predictable location. The starting material $Fe(CO)_2(NO)_2$ exhibits two nitrosyl stretches at 1797 and 1725 cm^{-1} and two carbonyl stretches at 2080 and 2018 cm^{-1}. Upon replacement of one of the carbonyls with a phosphine ligand, the ν_{NO} stretches shift to lower values in the region of 1750 to 1715 cm^{-1}, resulting from an increase in back-donation of electron density from the d-orbital of the metal center into the π^* orbital of the NO group. The replacement of the second carbonyl by the phosphine group causes a shift of both NO stretching frequencies to even lower wavenumbers in the range of 1650 to 1750 cm^{-1}, as listed in Table 1.

Interestingly, the disubstituted compounds **1** and **3** both shift to wavenumbers in the range of 1725-1720 cm^{-1} and 1675-1670 cm^{-1}, while compound **2** and a similar compound using 1,2-bis(diphenylphosphino)ethane (DPPE)[xix] exhibit an even greater shift in the range of 1708-1707 cm^{-1} and 1660-1657 cm^{-1}. This indicates that compound **2** and the DPPE complex both have N-O bonds that are weakened more than those of compounds **1** and **3** after substitution. This trend illustrates the fact that compound **2** and the DPPE compound have phosphorus atoms that act as stronger nucleophiles during the substitution reaction and are overall stronger σ-donors. Conversely, the ligands in **1** and **3** act as weaker nucleophiles, likely due to the presence of C=C π-bonds between the two phosphorus atoms. It is possible that the double bond allows for partial redistribution of the electron density from the two phosphorus atoms, leading to a lower amount of electron density available for donation from the phosphorus to the iron center and consequently, less back-donation from the metal to the NO group. This is also confirmed by the X-ray crystallographic analysis and the theoretical calculations, which will be discussed later.

UV-Vis Spectroscopy

The UV-Visible absorption spectra for complexes **1–3** show strong absorption peaks in the ultraviolet region around 248 nm, a shoulder from 275 to 320 nm, and a weaker broad peak from 475 to 600 nm. The UV region of the spectrum is several orders of magnitude more intense than the visible region. The peak at 248 nm has been assigned to $\pi - \pi^*$ transitions from the four phenyl rings of the ligand because the same absorption was also observed in the ligands alone. The shoulder from 275 to 320 nm in the UV region are possibly due to a metal to ligand charge transfer (MLCT), which is strong because the absorption is both spin-allowed and Laporte-allowed. The broad peaks from 475 to 600 nm in the visible region (Figure 1) are much weaker and could be attributed to d-d transitions, characteristic of transition metal compounds. Molar absorptivity calculations were done by taking the absorbance at the highest point of the broad peak at 505 nm at several concentrations. Plots of absorption vs concentration yielded the molar absorptivity coefficients of 184.6 M^{-1} cm^{-1}, 166.4 M^{-1} cm^{-1} and 241.4 M^{-1} cm^{-1} for complexes **1**, **2** and **3**, respectively. These values are typical for d-d transitions of transition metal complexes with tetrahedral geometry.

X-ray Crystallography

Single crystals of X-ray quality ranging in size from 1 mm^3 to 5 mm^3 were grown by allowing the solvent to slowly evaporate and the X-ray crystal structures of the chelated compounds **1–3** were determined by mounting a suitable single crystal on a glass fiber. Crystallographic collection and refinement parameters can be found in Table 2. Selected bond lengths and bond angles can be found in Table 3 and Table 4, respectively. All three compounds crystallized in the monoclinic crystal system, with space groups of P2(1)/c for compounds **1** and **2** and C2/c for **3**. The iron centers on all three crystalline compounds show the distorted tetrahedral geometry typical of DNIC species. The X-ray crystal structures are shown in Figures 2–4.

Compounds **1** and **3** consist of distorted five-membered rings formed by the Fe atom, two phosphorus atoms and two carbon atoms. This is to be expected since the sp^2 hybridization of the double bonded carbon backbones holds the phosphorus atoms at a rigid angle of 120°. Because of this geometry, both compounds exhibit P-Fe-P bonds that are less than 90° and Fe-P bond distances that are longer than a normal C-C single bond. Compound **2** consists of a six-membered ring containing three carbon atoms, two phosphorus atoms and the iron atom. By comparison, the two phosphorus atoms of the ligand in compound **2** are not held in a rigid orientation as the carbon chain connecting the phosphorus atoms contains three single-bonded carbons instead of two carbons with double bonds as in **1** and **3**. This allows for compound **2** to have a larger P-Fe-P bond angle of 94.45(3)°. However, the P-Fe bond lengths are similar to those of compounds **1** and **3** at ~2.2 Å. Compound **2** also exhibits a six-membered ring in a distorted chair conformation due to the contracted P-Fe-P bond angle.

Dinitrosyl iron complexes are frequently described as having "*attracto*" conformations where the N-Fe-N bond angles are generally less than or equal to 130° but are greater than the O-Fe-O bond angles.[xx] This conformation leads to the two oxygen atoms being slightly bent towards each other. The *attracto* conformation is usually observed in first-row transition metal complexes containing a good **π**-acceptor ligand. Compound **2** exhibits a N-Fe-N bond angle of 126.42(11)°, which is greater than the O-Fe-O bond angle of 124.47°. This compound exhibits the expected *attracto* conformation where the oxygen atoms are bent towards each other. This fact is reinforced upon considering that the Fe-N-O bond angles of the compound are 175–176°, which is close to linear, but still differs by 4–5°. On the contrary, compounds **1** and **3** have N-Fe-N bond angles of ~129° {129.46(8)° and 129.80(12)°}, O-Fe-O bond angles of ~130–131° and nearly linear Fe-N-O bond angles of 178–179°. This indicates that these two complexes are of the rarer "*repulso*" conformation. An exaggerated molecular illustration of the *attracto* and *repulso* conformations for these compounds is shown in Figure 5.

Typically, the *repulso* conformation is more common for the second-row and third-row transition metals.[xxi] For example, the N-M-N and O-M-O bond angles reported for $M(NO)_2(PPh_3)_2$ complex are 139.2° and 142.7° when M = Ru[xxii] and 139.1° and 140.6° when M = Os.[xxiii] This is also true for the cationic species, $[M(NO)_2(PPh_3)_2]^+$, where the

reported N-M-N and O-M-O bond angles are 157.5° and 173.7° for Rh and 154.2° and 167.5° for Ir, respectively.[xxiv]

In order to determine whether steric or electronic effects dictate the different conformations between *attracto* and *repulso*, another complex similar to compound **2** was examined. The compound $Fe(NO)_2(DPPE)$,[19] which differs from compound **2** by only one carbon atom, has a P2(1)/c space group similar to compound **1**. The N-O bond distances for this structure (1.185 and 1.200 Å) are very similar to those of the chelated structures synthesized in this work, while the Fe-N bonds (1.658 and 1.681 Å) are similar as well. This indicates that the DPPE ligand experiences back-donation in a similar manner to **1**, **2** and **3**. One difference lies in the angles of the iron atom and the NO groups. The N-Fe-N bond angle for the DPPE complex is 125.4° which is similar to compound **2**. However the O-Fe-O bond angle for the DPPE complex is given as 124.0°. These angles indicate that this complex is of the *attracto* conformation similar to **2**, despite the fact that it also contains a 5-membered ring like compounds **1** and **3**. The *repulso* conformations exhibited by compounds **1** and **3** are quite rare. Only one similar compound has been crystallized in the *repulso* conformation; $Co(NO)_2(DPPE)$ with a N-Co-N bond angle of 131.7° and an O-Co-O bond angle of 135.9°.[xxv]

When examining the IR stretching frequencies for compounds **2** and $Fe(NO)_2(DPPE)$, it can be seen that they both have similar values. Thus both phosphine ligands donate electron density in a manner that is more intense than the ligands containing **π**-bonds. Because compounds **1**, **3** and the DPPE complex all have five-membered rings, but **1** and **3** are *repulso* while the DPPE is *attracto*, the conformational preference cannot be due to a steric effect. The difference between the *attracto* and *repulso* forms must then be an electronic effect due to **1** and **3** containing C=C **π** bonds, while **2** and the DPPE complex do not.

The bond distances of the NO groups reveal yet more information about the nature of the phosphorus-iron bonds. The Fe-N bond distances at ~1.65 Å are contracted while the N-O bond distances of ~1.2 Å are slightly lengthened. This indicates that there is a significant amount of back-donation of electron density from the iron atom into the **π***-orbitals of the NO ligands. This supports the idea that the NO bonds are being weakened as shown by the IR spectral data mentioned earlier.

Cyclic Voltammetry

The redox behaviors of complexes **1–3** were studied through cyclic voltammetry as shown in Figure 6. The CV of each of the compounds was first compared with that of their respective ligand to identify whether any redox reactions are coming specifically from the ligand, and not the iron center. Compound **1** exhibits two quasi-reversible oxidations at 0.101 and 0.186 V. The separation between the two couples is small (0.086 V), but can still be distinguished visually. The presence of the two peaks can be verified by viewing the second derivative spectrum. Compound **2** exhibits a different behavior with two distinct and separate oxidation couples at 0.019 and 0.342 V. The separation between the two oxidation couples is quite large (0.323 V). The CV of compound **3** appears to have only one peak but the peak is broad and, by examining the second derivative CV, it can be confirmed that there

are actually two separate oxidation couples at 0.121 and 0.184 V. Table 5 summarizes the $E_{1/2}$ values for the three compounds.

The separations between the two oxidation couples $E°_{1/2}$ (1) and $E°_{1/2}$ (2) for complexes **1**, **2**, and **3** are 0.085, 0.323 and 0.063 V, respectively. It is found that the separation between redox couples for complexes **1** and **3** are much smaller than that of compound **2**, which is likely due to the structure of the chelating ligand, as compounds **1** and **3** both have C=C **π** bonds present while complex **2** does not. It is proposed that when the first oxidation occurs on the metal center, the positive charge can be delocalized through the C=C double bond into the chelating ligand itself, which makes the iron charge less than +1. As a result, the second oxidation would be easier, which renders the second oxidation $E°_{1/2}$ (2) to occur at a potential closer to the first oxidation $E°_{1/2}$ (1). As a consequence, the difference between the first oxidation and second oxidation is smaller. On the contrary, compound **2** lacks the **π** system and, therefore, cannot delocalize the charge away from the iron center. This means the iron has a full +1 charge, and removing a second electron from the iron center is more difficult. This is reflected by the second oxidation, which occurs at higher potential, resulting the larger separation between $E°_{1/2}$(2) and $E°_{1/2}$(1) values.

The CVs of variable scan rates from 100 mV to 900 mV were recorded for each compound and a plot of intensity of the current vs. the square root of the scan rate (Figure 7) shows a linear relationship indicating that all processes are diffusion-controlled single-electron redox couples.

Theoretical Calculations

B3LYP density functional theory calculations using the 6–31+G* basis set were carried out for each of the three compounds. In addition, B3LYP calculations using 6–31+G* and aug-cc-pVDZ basis sets were carried out for the model compounds, in which each of the phenyl groups on the phosphorus is replaced by a methyl group. The calculated bond lengths and bond angles matched well with the experimental data as shown in Tables 3 and 4. For compounds **1, 2** and **3**, the calculated average for the bond lengths of N-O using the 6–31+G* method are 1.1885, 1.1887 and 1.1862 Å, which are very close to the experimental averages, at 1.1875(2), 1.193(3) and 1.1865(3) Å, respectively. Using model compounds, the corresponding bond lengths are 1.1879, 1.1900 and 1.1876 Å for the 6–31+G* method and 1.1840, 1.1860 and 1.1836 Å for the aug-cc-pVDZ method, respectively. For Fe-N bond lengths, the average calculated values using the 6–31+G* method are 1.6376, 1.6373 and 1.6377 Å, which are systematically shorter than the average for the experimental ones {1.6446(17), 1.6495(2) and 1.651(2) Å} respectively. Using model compounds, the corresponding bond lengths are 1.6399, 1.6394 and 1.6396 Å for the 6–31+G* method and 1.6403, 1.6396 and 1.6400 Å for the aug-cc-pVDZ method, respectively, which are closer to the experimental values. The experimental average bond length for Fe-P is 2.2183(5), 2.2419(7) and 2.2297(7) Å, for compounds **1, 2** and **3**, while the corresponding calculated averages are 2.2380, 2.2430, and 2.2391 Å for the 6–31+G* method, 2.2113, 2.2149, and 2.2172 Å for the 6–31+G*(model), and 2.2324, 2.2404 and 2.2395 Å for the aug-cc-pVDZ(model) method, respectively. The aug-cc-pVDZ(model) produced best fit for

experimental data, where the average bond length of Fe-P is longer for **2** than that of **1** and **3**.

It is observed that the IR stretching frequencies for the NO group are 10–15 cm^{-1} lower for complex **2** than for complexes **1** and **3**, indicating stronger back donation from the DPPP ligand than DPPBz and DPPEt ligands. Our calculated harmonic frequencies, as shown in Table 1, are in good agreement with the trend in the IR frequencies. It should be noted that all calculated harmonic frequencies are about 5% higher than the corresponding experimental frequencies, which is typical because the unharmonicity correction would be expected to fill such a difference. The trend in the IR frequencies for the NO group is also consistent with the X-ray crystal structure data, where the average bond lengths for N-O is 1.193(3) Å for **2**, which is longer than that of **1** and **3** {1.1875(2) and 1.1865(3) Å, respectively}, because the back-donation weakens the N-O bond. The calculated data using all three methods consistently showed that the bond lengths of the N-O group are longer for compound **2** than that of compound **1** and **3**.

The calculated bond angles that dictates the local geometry of the metal center, such as P-Fe-P and P(1,2)-Fe-N(1,2) match well with the experimental data. The experimental average of the Fe-N-O angles are 178.56° and 179.05° for compound **1** and **3**, which are more linear than that of compound **2** (176.18°). The calculated average Fe-N-O angles using 6–31+G* are 177.43°, 176.83° and 176.80° for **1**, **2** and **3**, respectively. When using the model compounds, the average bond angles are 179.21°, 179.43° and 179.04° for the 6–31+G* method and 178.70°, 178.81° and 178.51° for the aug-cc-pVDZ method for **1**, **2** and **3**, respectively. The calculated bond angles of N-Fe-N and O-Fe-O are quite similar for the three compounds and only *attracto* conformations are predicted, while experimentally **2** exhibits *attracto* but **1** and **3** possess *repulso* conformations.

The highest occupied molecular orbital (HOMO) - lowest unoccupied molecular orbital (LUMO) energy separations are obtained from the calculations as well. The HOMO-LUMO gaps for compounds **1, 2** and **3** are 3.736, 4.060, and 3.669 eV, respectively. It is interesting to note that these HOMO-LUMO gaps are very large, which makes the compounds very stable with respect to reduction, thus may account for the fact that only oxidations are observed in the electrochemical study.

It is also noted that the compounds **1** and **3** are similar, while compound **2** is significantly larger. It is consistent with the fact that the observed charge transfer bands at ~320 nm in the UV-Vis spectra {Figure 1(a)} have similar intensity for compounds **1** and **3**, but are much stronger for compound **2**. From the experimental and calculated bond lengths and FT-IR data, it is clear that the DPPP ligand acts as better donor to the metal, thus the metal has more electrons available for back-donation for compound **2** than compounds **1** and **3**. It has been reported that depleting electron density from the metal center through metal to ligand back-bonding results in widening the HOMO-LUMO gap,[xxvi] which is consistent with our results. Moreover, it is known that the HOMO-LUMO gap is lowered by the presence of conjugated π-systems in organic molecules.[xxvii] Therefore, the double bond in between the two phosphorus atoms may account for the lower HOMO-LUMO gap for compounds **1** and **3**.

CONCLUSIONS

We have demonstrated that dinitrosyl iron complexes containing chelated structures of phosphine ligands including 1,2-bis(diphenylphosphino)benzene, cis-1,2-bis(diphenylphosphino)ethylene and 1,3-bis(diphenylphosphino)propane, can be synthesized and characterized by IR, UV-Vis, NMR, X-ray and CV methods.

Infrared spectroscopy was used to qualitatively monitor the reaction progress. The reaction times were found to be dependent on the presence of coordinating and non-coordinating solvents. The first substitution occurred over one hour in THF vs. 24 hours in dichloromethane, indicating that THF may act as a hard base and stabilizes the loss of the first carbonyl group.

Single crystals of compounds **1**, **2** and **3** were obtained and the X-ray crystallographic data shows they crystallize in the monoclinic crystal system with P2(1)/c, P2(1)/c and C2/c space groups and the unit cells contain 4, 4 and 8 molecules, respectively. The average Fe-N-O bond angles for the three compounds are all close to linear with compounds **1** and **3** at 178.5° while compound **2** at 175.5°, which is smaller. Compounds **1** and **3** possess five-membered rings and have P-Fe-P bond angles less than 90° while compound **2** has an angle of 94° and contains a six-membered ring. Complex **2** exhibits the *attracto* state while **1** and **3** exhibit the *repulso* conformations, which is rare for the first row transition metals. The presence of **π**-bonds on the carbon bridge of the bis(diphenyl)phosphine ligands plays a significant role in the observed conformation, while steric hindrance is eliminated as a cause.

The UV-Visible absorption spectra for complexes **1–3** show strong absorptions at 248 nm, a shoulder from 275 to 320 nm, and a weaker broad peak from 475 to 600 nm, which are assigned to **π** – **π*** transitions from the four phenyl rings of the ligand, metal to ligand charge transfer (MLCT), and d-d transitions, respectively. Molar absorptivity coefficients for the visible spectra are calculated to be 184.6 M^{-1} cm^{-1}, 166.4 M^{-1} cm^{-1} and 241.4 M^{-1} cm^{-1} for complexes **1**, **2** and **3**, respectively, which are typical for d-d transitions of transition metal complexes with tetrahedral geometry.

The redox behaviors of all three compounds were studied through cyclic voltammetry. All three compounds in the series exhibit two quasi-reversible oxidation peaks. The $E°_{1/2}$ values for compounds **1**, **2** and **3** are 0.101 and 0.186 V, 0.121 and 0.184, and 0.019 and 0.342V, respectively. The separation between the two oxidation couples is much smaller for compounds **1** and **3** when compared with that of compound **2**, which has been attributed to the presence of **π** -bonds in the bisphosphine chelating ligands, allowing for charge delocalization upon the first oxidation occurring.

DFT calculations using the B3LYP functional and the 6–31+G* basis set were performed on all three compounds. In addition, B3LYP calculations using the 6–31+G* and aug-cc-pVDZ basis sets were carried out for the model compounds, in which each of the phenyl groups on the phosphorus is replaced by a methyl group. The calculated bond lengths and angles match well with the experimental data and the calculated IR stretching frequencies are also consistent with experimental observations. The calculated HOMO-LUMO gaps for

compounds **1, 2** and **3** are 3.736, 4.060, and 3.669 eV, respectively. The higher HOMO-LUMO gap for compound **2** is consistent with more electron back-donation from the metal to the NO ligands, while the lower HOMO-LUMO gaps for compounds **1** and **3** are attributed to the conjugated **π**-systems on the DPPBz and DPPEt ligands. These large HOMO-LUMO gaps are also consistent with the lack of the usual reductions in electrochemical studies.

Supplementary Material

Refer to Web version on PubMed Central for supplementary material.

Acknowledgments

We wish to thank the National Institute of Health (NIH) MBRS SCORE Program (Grant #1SC3GM092301-01) for financial support.

List of References

i. (a) Feldman PL, Griffith OW, Stuehr DJ. Chem. Eng. News. Dec. 1993; 20:26–38.(b) Koshland OE Jr. Science. 1992; 258:1861–1865. [PubMed: 1470903] (c) Foster MW, Cowan JA. J. Am. Chem. Soc. 1999; 121:4093–4100.(d) Walker, FA.; Ribeiro, JMC.; Montfort, WR. Metals in Biological Systems. Sigel, H.; Sigel, A., editors. Vol. 36. New York: Marcel Dekker; 1998. p. 619-661.

ii. (a) Lancaster JR Jr, Hibbs JB Jr. Proc. Natl. Acad. Sci. USA. 1990; 87:1223–1227. [PubMed: 2153975] (b) Vanin AF, Varich VW. Stud. Biophys. 1981; 86:177–179.(c) Rogers PA, Ding H. J. Biol. Chem. 2001; 276:30980–30986. [PubMed: 11423535] (d) Butler AR, Megson IL. Chem. Rev. 2002; 102:1155–1166. [PubMed: 11942790] (e) Weiss G, Goossen B, Doppler W, Fuchs D, Pantopoulos K, Werner-Felmayer G, Wachter H, Hentze MW. EMBO J. 12(193):3651–3657. [PubMed: 7504627] (f) Ding H, Demple B. Proc. Natl. Acad. Sci. U.S.A. 2000; 97:5146–5150. [PubMed: 10805777] (g) Mulsch A, Mordintecv P, Vanin AF, Busse R. FEBS Lett. 1991; 294:252–256. [PubMed: 1684553]

iii. (a) Muller B, Kleschyov AL, Stoclet JC. Brit. J. Pharm. 1996; 119:1281–1285.(b) Lee M, Arosio P, Cozzi A, Chasteen ND. 1994; 33:3679–3687.

iv. (a) Lo FC, Chen CL, Lee CM, Tsai MC, Lu TT, Liaw WF, Yu SF. J. Biol. Inorg. Chem. 2008; 13:961–972. [PubMed: 18449575] (b) Rogers PA, Eide L, Klungland A, Ding H. DNA Repair. 2003; 2:809–817. [PubMed: 12826281] (c) Lewandowska H, Brzóska K, Meczyńska-Wielgosz S, Rumianek K, Wójciuk G, Kruszewski M. Postepy Biochem. 2010; 56:298–304. [PubMed: 21117318]

v. (a) Drapier JC, Pellat C, Henry Y. J. Biol. Chem. 1991; 266:10162–10167. [PubMed: 1645341] (b) Vanin AF. Open Conf. Proc. J. 2013; 4:47–53.(c) Poelhsitza GV, Bogadoa AL, de Araujob MP, Selistre-de-Araújoc HS, Ellenad J, Castellanod EE, Batistaa AA. Polyhedron. 2007; 26:4707–4712.

vi. (a) Tonzetich ZJ, Heroguel F, Do LH, Lippard SJ. Inorg. Chem. 2011; 50:1570–1579. [PubMed: 21244036] (b) Chen YJ, Ku WC, Feng LT, Tsai ML, Hsieh CH, Hsu WH, Liaw WF, Hung CH. J. Am. Chem. Soc. 2008; 130:10929–10938. [PubMed: 18661983] (c) Hsieh CH, Darensbourg MY. J. Am. Chem. Soc. 2010; 132:14118–14125. [PubMed: 20857969] (d) Holloway LR, Li L. Struct. Bond. 2013; 101:101.(e) Richter-Addo GB, Legzdins P, Burstyn J. Chem. Rev. 2002; 102:857–1066. [PubMed: 11942780]

vii. (a) Ford PC, Bourassa J, Miranda K, Lee B, Lorkovic I, Boggs S, Kudo S, Laverman L. Coord. Chem. Rev. 1998; 171:185–202.(b) Works CF, Ford PC. J. Am. Chem. Soc. 2000; 122:7592–7593.(c) Wang PG, Xian M, Tang X, Wu X, Wen Z, Cai T, Janczuk AJ. Chem. Rev. 2002; 102:1091–1134. [PubMed: 11942788] (d) Madhani M, Patra AK, Miller TW, Eroy-Reveles AA, Hobbs A, Fukuto JM, Mascharak PK. J. Med. Chem. 2006; 49:7325–7330. [PubMed: 17149862]

(e) Bourassa J, DeGraff W, Kudo S, Wink DA, Mitchell JB, Ford PC. J. Am. Chem. Soc. 1997; 119:2853–2860.(f) De Leo M, Ford PC. J. Am. Chem. Soc. 1999; 121:1980–1981.

viii. Dogan J, Schulte JB, Swiegers GF, Wild SBJ. Org. Chem. 2001; 65:951.

ix. (a) Jones MW, Powell DR, Richter-Addo GB. Acta Cryst. 2011; 67:332.(b) Li L. Comm. Inorg. Chem. 2002; 23:335–353.

x. (a) McBride DW, Stafford SL, Stone GFA. Inorg. Chem. 1962; 1:386.(b) Griffith WP. Adv. Organomet. Chem. 1968; 7:211.

xi. (a) Wang R, Wang X, Sundberg EB, Nguyen P, Grant GPG, Sheth C, Zhao Q, Herron S, Kantardjieff KA, Li L. Inorg. Chem. 2009; 48:9779–9785. [PubMed: 19769382] (b) Wang R, Xu W, Zhang J, Li L. J. Mol. Struc. 2009; 923:110–113.

xii. Li L, Reginato N, Urschey M, Stradiotto M, Liarakos JD. Can. J. Chem. 2003; 81:468–475.

xiii. Heiber W, Beutner H. Anorg. Allgem. Chem. 1963; 320:101.

xiv. F. Seel Handbook of Preparative Inorganic Chemistry. New York NY: Academic Press Inc.; 1965. p. 1760

xv. (a) SMART and SAINT for Windows NT Software Reference Manuals v. 5.0. Madison, WI, USA: Bruker Analytical X-Ray Instrument Inc.; 1997. (b) Sheldrick, GM. SADABS – A software for Empirical Absorption Correction. Germary: University of Göttingen; 1997. (c) SHELXTL Reference Mabual, Version 5.1. Madison, WI: Bruker Analytical X-Ray System; 1997.

xvi. (a) Becke AD. Phys. Rev. A. 1988; 38:3098. [PubMed: 9900728] (b) Perdew JP, Wang Y. Phys. Rev. B. 1992; 45:13244.(c) Becke AD. J. Chem. Phys. 1993; 98:5648.(d) Krishnan R, Binkley JS, Seeger R, Pople JA. J. Chem. Phys. 1980; 72:650.

xvii. Frisch, MJ.; Trucks, GW.; Schlegel, HB.; Scuseria, GE.; Robb, MA.; Cheeseman, JR.; Scalmani, G.; Barone, V.; Mennucci, B.; Petersson, GA.; Nakatsuji, H.; Caricato, M.; Li, X.; Hratchian, HP.; Izmaylov, AF.; Bloino, J.; Zheng, G.; Sonnenberg, JL.; Hada, M.; Ehara, M.; Toyota, K.; Fukuda, R.; Hasegawa, J.; Ishida, M.; Nakajima, T.; Honda, Y.; Kitao, O.; Nakai, H.; Vreven, T.; Montgomery, JA., Jr; Peralta, JE.; Ogliaro, F.; Bearpark, M.; Heyd, JJ.; Brothers, E.; Kudin, KN.; Staroverov, VN.; Kobayashi, R.; Normand, J.; Raghavachari, K.; Rendell, A.; Burant, JC.; Iyengar, SS.; Tomasi, J.; Cossi, M.; Rega, N.; Millam, NJ.; Klene, M.; Knox, JE.; Cross, JB.; Bakken, V.; Adamo, C.; Jaramillo, J.; Gomperts, R.; Stratmann, RE.; Yazyev, O.; Austin, AJ.; Cammi, R.; Pomelli, C.; Ochterski, JW.; Martin, RL.; Morokuma, K.; Zakrzewski, VG.; Voth, GA.; Salvador, P.; Dannenberg, JJ.; Dapprich, S.; Daniels, AD.; Farkas, Ö.; Foresman, JB.; Ortiz, JV.; Cioslowski, J.; Fox, DJ. Gaussian 09, Revision D.01. Wallingford CT: Gaussian, Inc.; 2009.

xviii. (a) Basolo F. Polyhedron. 1990; 9:1503.(b) Morris DE, Basolo F. J. Am. Chem. Soc. 1969; 90:2536.

xix. Li Kam Wah H, Postel M. Inorg. Chim. Acta. 1989; 165:215.

xx. Richter-Addo GB, Legzdins P. Metal Nitrosyls. 1992; Ch. 5

xxi. Martin RL, Taylor D. Inorg. Chem. 1976; 15:2970–2976.

xxii. (a) Gaughan AP, Corden BJ, Eisenberg R, Ibers JA. Inorg. Chem. 1974; 13:786–791.(b) Bhaduri S, Sheldrick GM. Acta Crystallogr. Sect E. 1975; 31:897.

xxiii. Haymore BL, Ibers JA. Inorg. Chem. 1975; 14:2610–2617.

xxiv. (a) Mingos DMP, Ibers JA. Inorg. Chem. 1970; 9:1105–1111.(b) Kaduk JA, Ibers JA. Inorg. Chem. 1975; 14:3070–3073.

xxv. Kadnk JA, Ibers JA. Inorg. Chem. 1977; 16:3283.

xxvi. Melissa V, Werrett D, Chartrand D, Gale JD, Hanan GS, MacLellan JG, Massi M, Muzzioli S, Raiteri P, Skelton BW, Silberstein M, Stagni S. Inorg. Chem. 2011; 50:1229–1241. 1229. [PubMed: 21268651]

xxvii. (a) Aihara JI. J. Phys. Chem. A. 1999; 103:7487–7495.(b) Ruiz-Morales Y. J. Phys. Chem. A. 2002; 106:11283–11308. 2002.

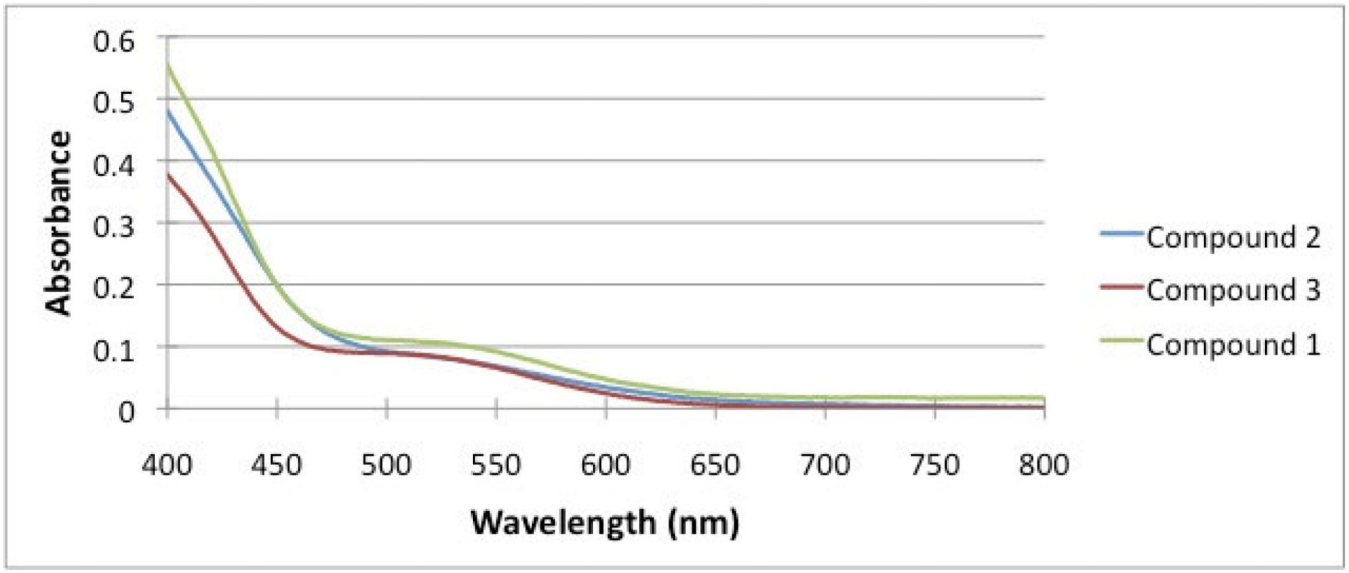

Figure 1.
UV-Vis spectra for compounds **1**, **2** and **3** in the visible region.

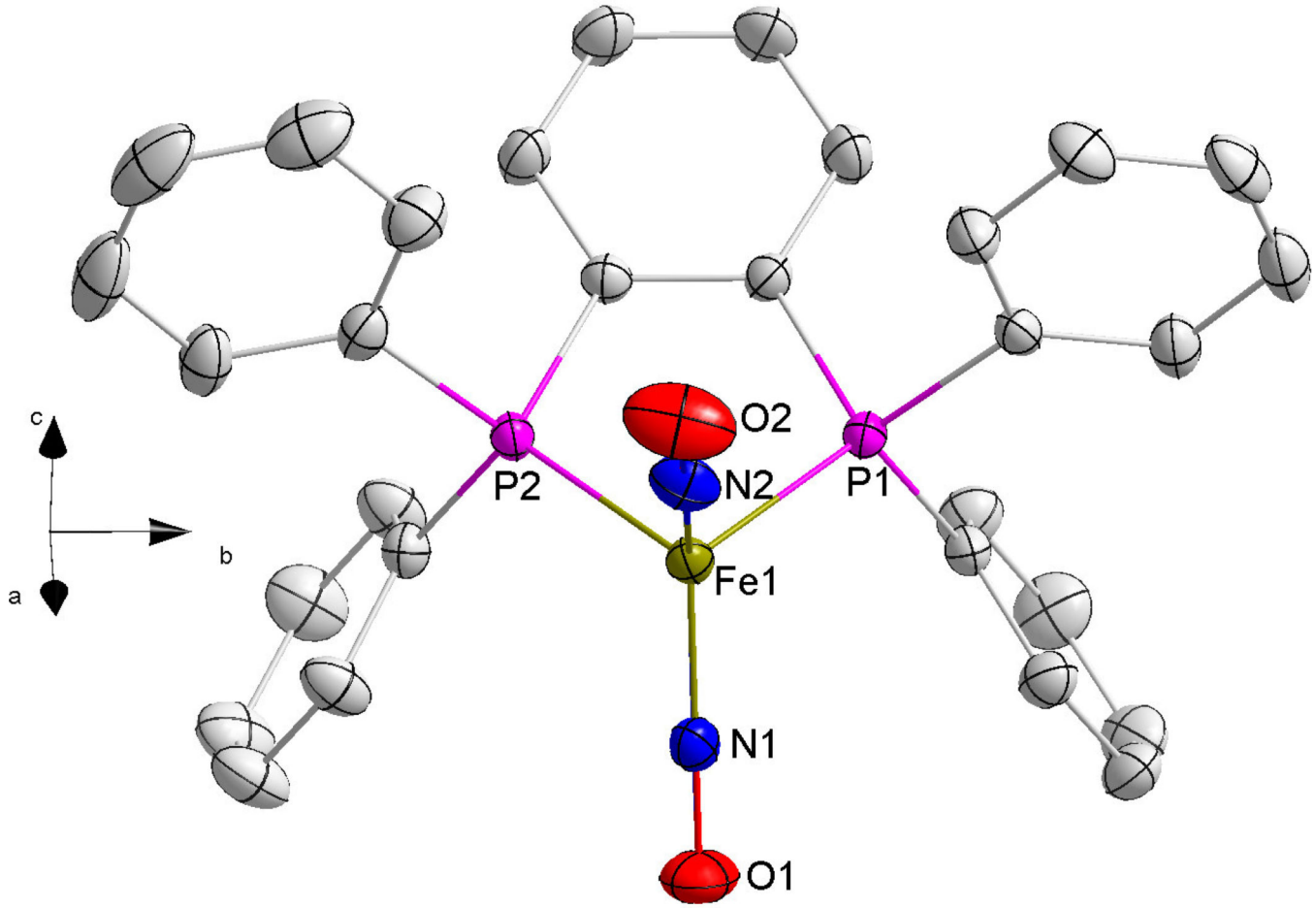

Figure 2.
An ORTEP image of compound **1** with thermal ellipsoids drawn at 50% probability. For clarity, hydrogen atoms on the carbon rings have been removed.

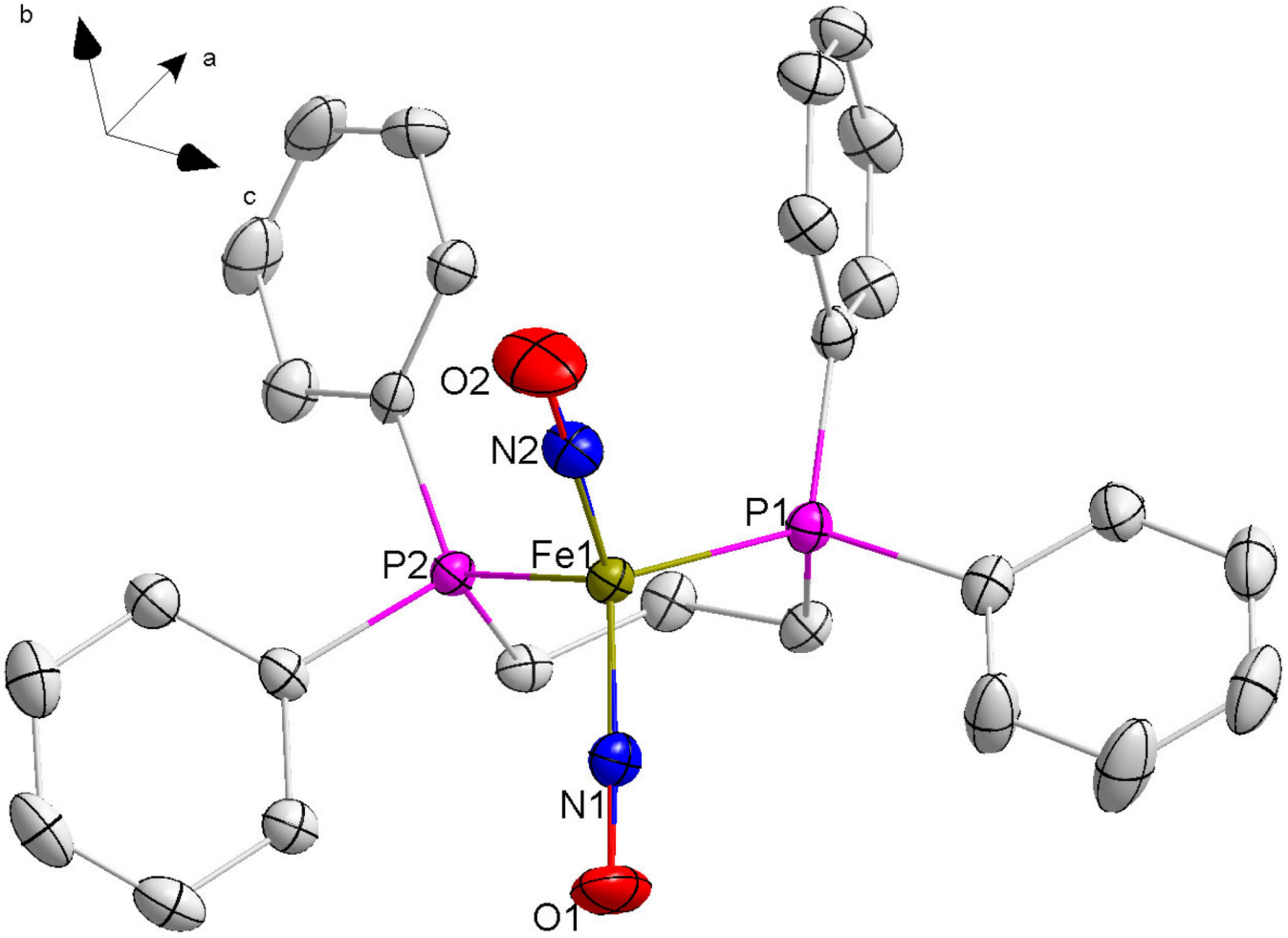

Figure 3.

An ORTEP image of compound **2** with thermal ellipsoids drawn at 50% probability. For clarity, hydrogen atoms on the carbon rings have been removed.

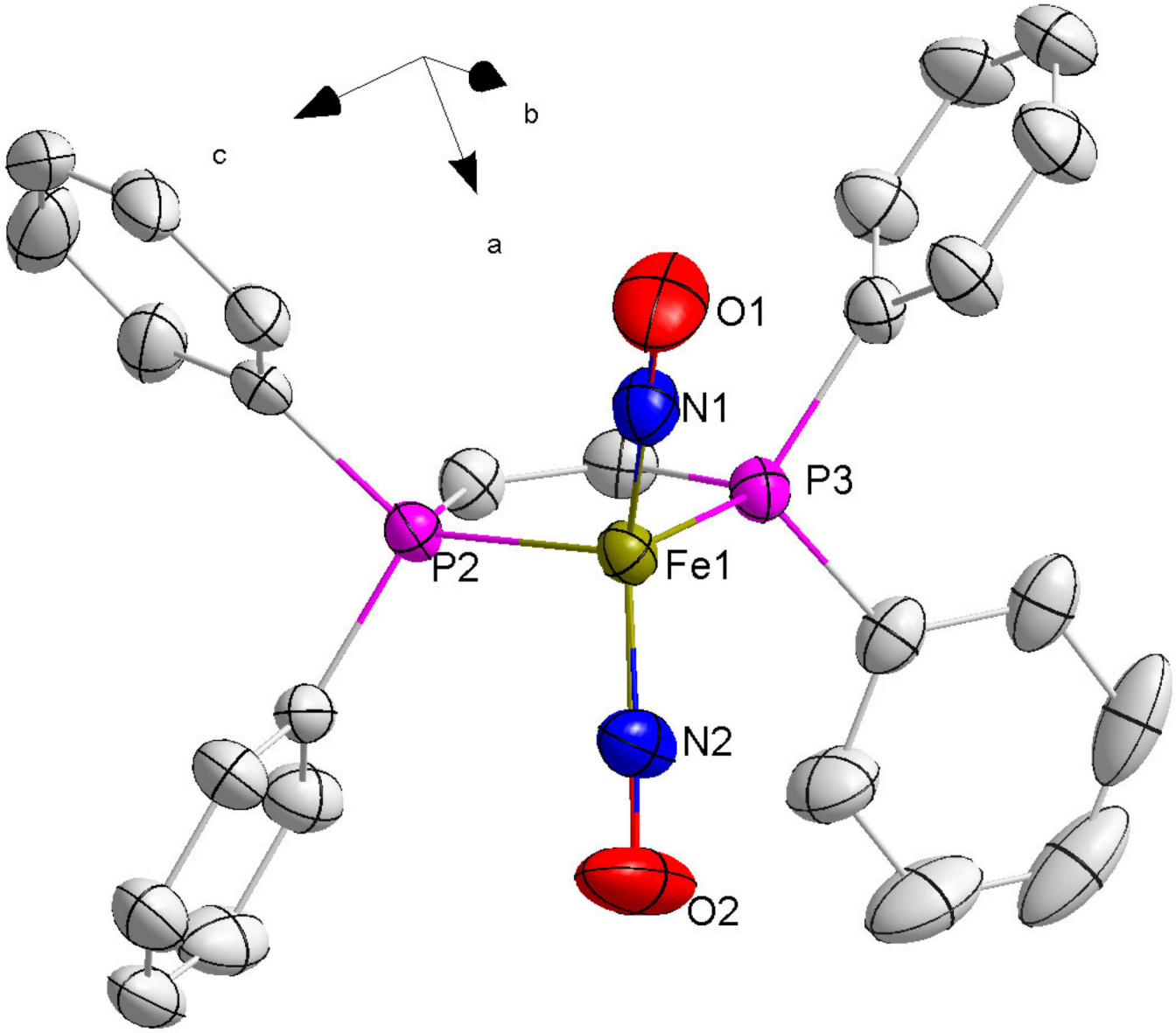

Figure 4.

An ORTEP image of compound **3** with thermal ellipsoids drawn at 50% probability. For clarity, hydrogen atoms on the carbon rings have been removed.

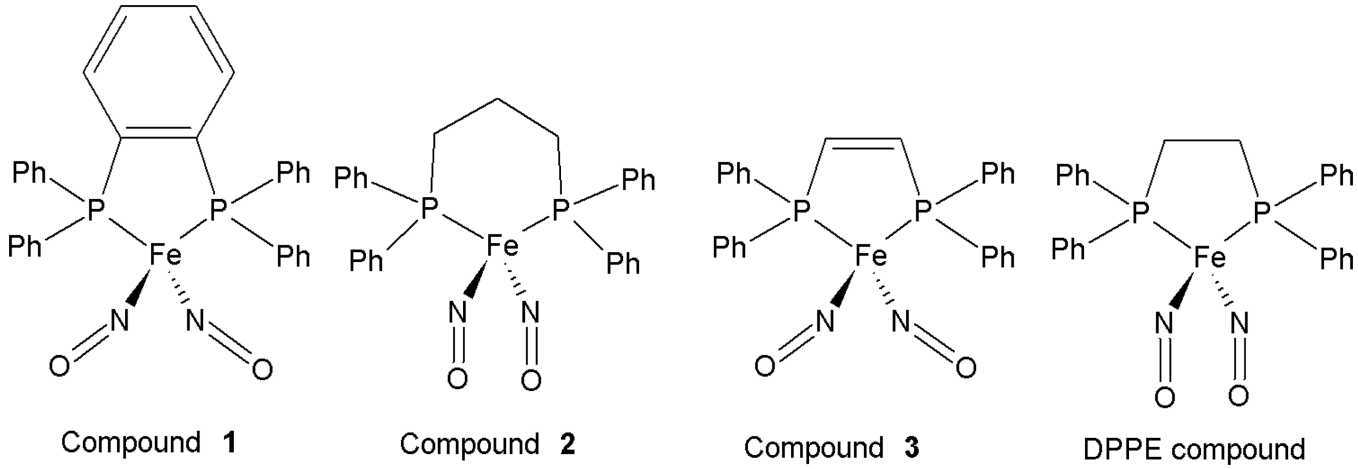

Figure 5.

Molecular drawing illustrates the "*attracto*" and "*repulso*" conformations for compounds **1–3** and a similar compound $Fe(NO)_2$(DDPE).

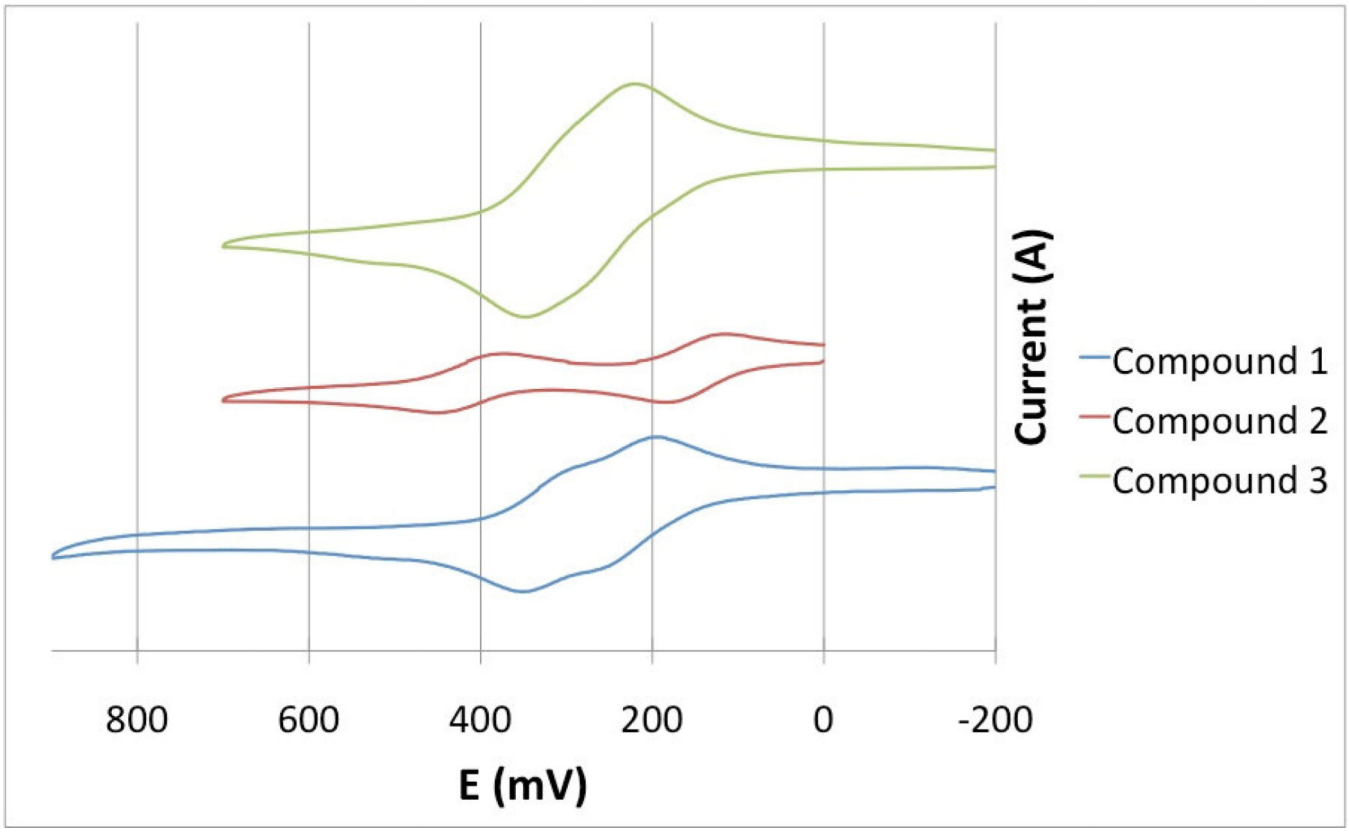

Figure 6.

Cyclic voltammograms of compounds **1**, **2** and **3** a scan rate of 100 mVs^{-1} in CH_2Cl_2 solution containing 0.1 M TBAP.

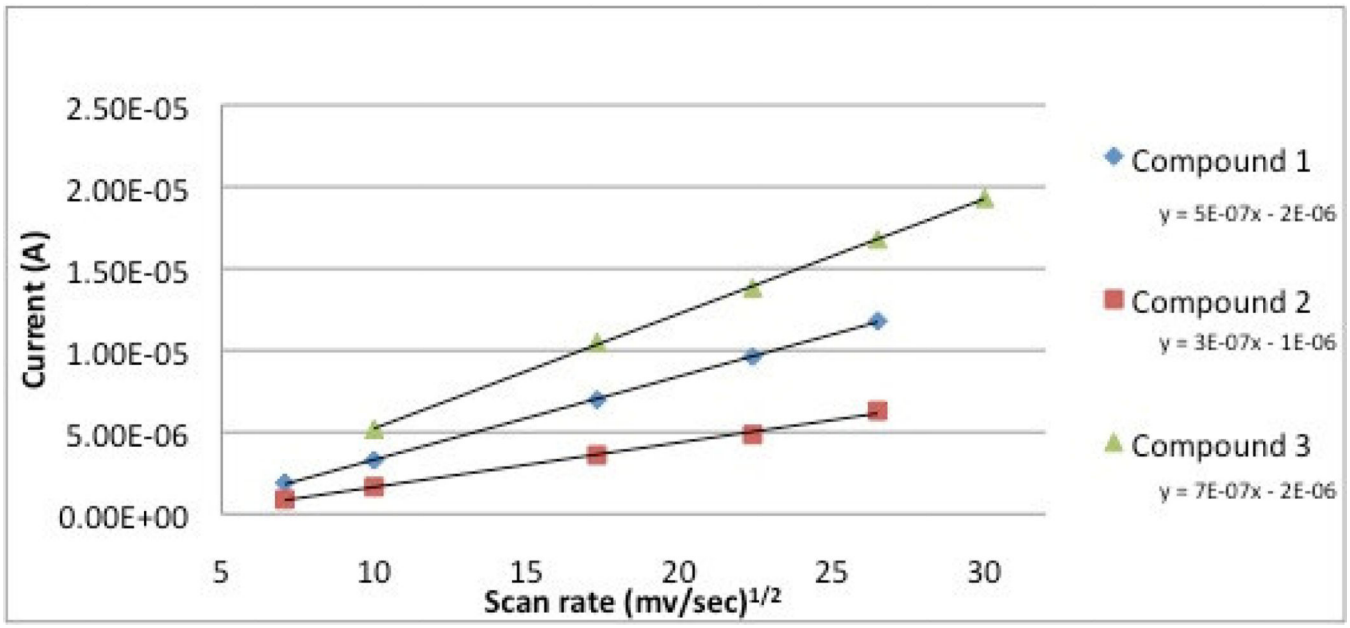

Figure 7.
Plot of current vs (scan rate)$^{1/2}$.

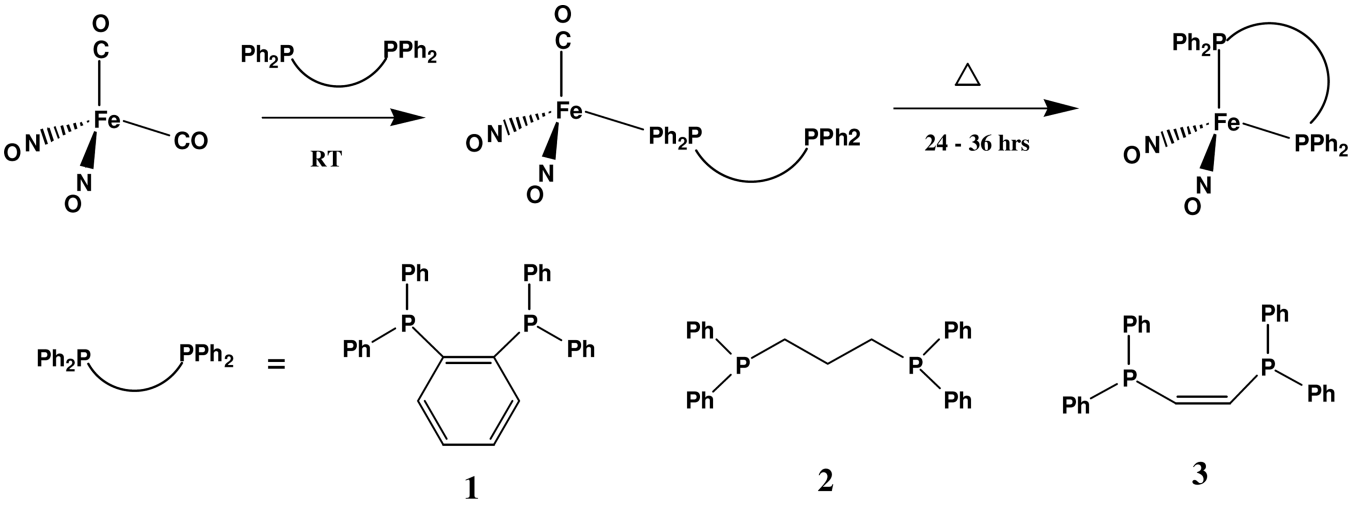

Scheme 1.

Synthesis of mono-substituted and double-substituted chelating compounds **1–3**.

Table 1

List of Experimental and Calculated IR Stretching Frequencies for CO and NO.

Compounds	ν_{CO} (cm^{-1})	ν_{NO} (cm^{-1})	References
$Fe(CO)_2(NO)_2$	2080 and 2018	1797 and 1725	This work
$Fe(NO)_2(CO)$(DPPBe)	1994	1760, 1719[a]	This work
$Fe(NO)_2$(DPPBe) (**1**)	-	1719, 1675[a]	This work
	-	*1814, 1763*[d]	This work
$Fe(NO)_2(CO)$(DPPPr)	2002	1759, 1716[a]	This work
$Fe(NO)_2$(DPPPr) (**2**)	-	1708, 1660[b]	This work
	-	*1807, 1756*[d]	This work
$Fe(NO)_2(CO)$(DPPEt)	2001	1758, 1716[a]	This work
$Fe(NO)_2$(DPPEt) (**3**)	-	1723, 1674[b]	This work
	-	*1825, 1760* [d]	This work
$Fe(NO)_2(CO)P(C_6H_5)_3$	2009	1764, 1722	10
$Fe(NO)_2[P(C_6H_5)_3]_2$	-	1724, 1678	5
$Fe(NO)_2$(DPPE)	-	1707, 1657	10

(a)- in THF at room temperature

(b)- in dichloromethane at room temperature

*(c)*Solid KBr Pellet.

*(d)*Calculated frequencies using the B3LYP/6–31+G(d) method.

Table 2

Crystallographic Collection and Refinement Parameters for **1, 2** and **3**.

Parameter	Compound 1	Compound 2	Compound 3
Empirical Formula	C_{30} H_{24} Fe N_2 O_2 P_2	C_{27} H_{26} Fe N_2 O_2 P_2	C_{26} H_{22} Fe N_2 O_2 P_2
Molecular Weight	562.30	528.29	512.25
Description	Dark Purple Prism	Red needle	Dark Purple Plate
Size mm^3	4.0 × 0.4 × 0.3 mm^3	3.0 × 3.0 × 0.4 mm^3	5.0 × 3.0 × 2.0 mm^3
Temperature, K	230(2) K	296(2) K	296(2) K
Wavelength, Å	0.71073 Å	0.71073 Å	0.71073 Å
Crystal System	Monoclinic	Monoclinic	Monoclinic
Space group	P2(1)/c	P2(1)/c	C2/c
a, Å	9.9462(11) Å	9.4281(3) Å	17.9383(6) Å
b, Å	15.4195(17) Å	15.9709(6) Å	14.6440(6) Å
c, Å	17.828(2) Å	16.7774(7) Å	18.8183(6) Å
α, deg	90°	90°	90°
β, deg	92.218(5)°	93.437(2)°	95.914(2)°
γ, deg	90°	90°	90°
Volume $Å^3$	2732.1(5) $Å^3$	2521.72(16) $Å^3$	4917.0(3) $Å^3$
Z	4	4	8
Calc. Density mg/m^3	1.367 Mg/m^3	1.392 Mg/m^3	1.384 Mg/m^3
Abs. Coeff. mm^{-1}	0.699 mm^{-1}	0.752 mm^{-1}	0.769 mm^{-1}
F(000)	1160	1096	2112
θ Range deg.	1.75 to 25.15°	1.76 to 25.05°	1.80 to 25.01°
Index Ranges	−10<=h<=11 −18<=k<=18 −21<=l<=20	−11<=h<=11 −18<=k<=13 −18<=l<=19	−21<=h<=17 −14<=k<=17 −22<=l<=22
No. Refl. Coll.	31834	11208	8472
No. Indep. Refl.	4883 [R(int) = 0.0211]	4442 [R(int) = 0.0209]	4315 [R(int) = 0.0253]
Data / restr. / param	4883 / 0 / 430	4442 / 0 / 411	4315 / 0 / 386
Goodness-of-fit on F^2	1.000	1.063	1.006
Final R indices [I>2sigma(I)]	R1 = 0.0291, wR2 = 0.0843	R1 = 0.0348, wR2 = 0.0842	R1 = 0.0367, wR2 = 0.0944
R indices (all data)	R1 = 0.0357, wR2 = 0.0909	R1 = 0.0433, wR2 = 0.0905	R1 = 0.0513, wR2 = 0.1035
Largest diff. peak and hole	0.431 and −0.181 e.$Å^{-3}$	0.338 and −0.233 e.$Å^{-3}$	0.469 and −0.219 e.$Å^{-3}$

Table 3

List of Selected Experimental and Calculated Bond Lengths (Å) for Compounds **1, 2** and **3**.

Bond	Method	Compound 1	Compound 2	Compound 3
Fe(1)-N(1)	Expt	1.6485(16)	1.652(2)	1.650(2)
	6–31+G*	1.6373	1.6379	1.6389
	6–31+G*(model)	1.6399	1.6397	1.6396
	aug-cc-pVDZ(model)	1.6403	1.6398	1.6400
N(1)-O(1)	Expt	1.182(2)	1.190(3)	1.186(3)
	6–31+G*	1.1910	1.1881	1.1817
	6–31+G*(model)	1.1879	1.1903	1.1875
	aug-cc-pVDZ(model)	1.1840	1.1864	1.1836
Fe(1)-N(2)	Expt	1.6404(17)	1.647(2)	1.652(2)
	6–31+G*	1.6368	1.6366	1.6365
	6–31+G*(model)	1.6399	1.6390	1.6396
	aug-cc-pVDZ(model)	1.6403	1.6394	1.6400
N(2)-O(2)	Expt	1.193(2)	1.196(3)	1.187(3)
	6–31+G*	1.1859	1.1892	1.1907
	6–31+G*(model)	1.1879	1.1896	1.1875
	aug-cc-pVDZ(model)	1.1840	1.1856	1.1836
Fe(1)-P(1)	Expt	2.2180(5)	2.2501(7)	2.2228(7)
	6–31+G*	2.2378	2.2364	2.2407
	6–31+G*(model)	2.2112	2.2194	2.2172
	aug-cc-pVDZ(model)	2.2324	2.2404	2.2395
Fe(1)-P(2)	Expt	2.2185(5)	2.2336(7)	2.2297(7)
	6–31+G*	2.2382	2.2496	2.2375
	6–31+G*(model)	2.2114	2.2194	2.2172
	aug-cc-pVDZ(model)	2.2324	2.2404	2.2395

Table 4

List of Selected Experimental and Calculated Bond Angles (deg) for Compounds **1**, **2** and **3**.

Bonds		Compound 1	Compound 2	Compound 3
N(1)-Fe(1)-N(2)	Expt	129.46(8)	126.42(11)	129.80(12)
	6–31+G*	123.76	123.89	122.47
	6–31+G*(model)	126.44	127.59	126.31
	aug-cc-pVDZ(model)	125.82	126.81	125.68
P(1)-Fe(1)-P(2)	Expt	86.67(2)	94.45(3)	86.28(3)
	6–31+G*	86.17	96.33	87.44
	6–31+G*(model)	88.08	96.62	87.56
	aug-cc-pVDZ(model)	87.54	95.70	87.02
O(1)-Fe(1)-O(2)	Expt	131.17	124.47	130.31
	6–31+G*	121.61	121.46	119.80
	6–31+G*(model)	125.78	127.11	125.50
	aug-cc-pVDZ(model)	124.73	125.81	124.44
Fe(1)-N(1)-O(1)	Expt	178.90	176.68	179.50
	6–31+G*	176.92	176.36	177.52
	6–31+G*(model)	179.22	179.74	179.04
	aug-cc-pVDZ(model)	178.73	179.27	178.51
Fe(1)-N(2)-O(2)	Expt	178.23	175.67	178.6
	6–31+G*	177.94	176.97	176.08
	6–31+G*(model)	179.20	179.12	179.04
	aug-cc-pVDZ(model)	178.66	178.35	178.51
N(1)-Fe(1)-P(1)	Expt	109.33(5)	106.49(8)	112.33(8)
	6–31+G*	110.62	103.29	107.39
	6–31+G*(model)	108.86	106.11	109.03
	aug-cc-pVDZ(model)	109.12	106.18	109.34
N(1)-Fe(1)-P(2)	Expt	107.61(5)	100.48(7)	107.64(8)
	6–31+G*	110.63	109.31	107.37
	6–31+G*(model)	108.84	106.11	109.03
	aug-cc-pVDZ(model)	109.12	106.17	109.33
N(2)-Fe(1)-P(1)	Expt	106.66(6)	112.48(8)	102.08(8)
	6–31+G*	109.64	110.52	113.67
	6–31+G*(model)	108.94	108.04	109.03
	aug-cc-pVDZ(model)	109.27	108.79	109.33
N(2)-Fe(1)-P(2)	Expt	108.75(6)	111.32(8)	110.07(9)
	6–31+G*	109.64	109.82	112.84
	6–31+G*(model)	108.95	108.04	109.03
	aug-cc-pVDZ(model)	109.27	108.77	109.33

Table 5

List of Redox Potentials for Compounds **1**, **2** and **3**, their Cathodes and Anodes Peak Separations.

Compounds	**$E°_{1/2}(1)$ (V)[a]**	**$E°_{1/2}(2)$ (V)[a]**	**ΔE(1) (mV)[b]**	**ΔE(2) (mV)[b]**	**$[E°_{1/2}(2) - E°_{1/2}(1)]$ (mV)**
Ferrocene	0.132	-	89	-	
1	0.101	0.186	73	64	85
2	0.019	0.342	63	79	323
3	0.121	0.184	69	65	63

[a] Values corrected using the $E_{1/2}$ value of ferrocene/ferrocenium as a standard.

[b] ΔE(1) = Epa – Epc for $E°_{1/2}(1)$; ΔE(2) = Epa –Epc for $E°_{1/2}(2)$.